

Learning Latent Graph Dynamics for Deformable Object Manipulation

Xiao Ma, David Hsu, Wee Sun Lee
National University of Singapore
xiao-ma@comp.nus.edu.sg

Abstract—Manipulating deformable objects, such as cloth and ropes, is a long-standing challenge in robotics: their large degree of freedom (DoFs) and complex non-linear dynamics make motion planning extremely difficult. This work aims to learn latent *Graph dynamics for DefOrmable Object Manipulation* (G-DOOM). To tackle the challenge of many DoFs and complex dynamics, G-DOOM approximates a deformable object as a sparse set of interacting *keypoints* and learns a *graph neural network* that captures abstractly the geometry and interaction dynamics of the keypoints. Further, to tackle the perceptual challenge, specifically, object self-occlusion, G-DOOM adds a recurrent neural network to track the keypoints over time and condition their interactions on the history. We then train the resulting recurrent graph dynamics model through contrastive learning in a high-fidelity simulator. For manipulation planning, G-DOOM explicitly reasons about the learned dynamics model through model-predictive control applied at each of the keypoints. We evaluate G-DOOM on a set of challenging cloth and rope manipulation tasks and show that G-DOOM outperforms a state-of-the-art method. Further, although trained entirely on simulation data, G-DOOM transfers directly to a real robot for both cloth and rope manipulation in our experiments. A demonstration video is available at <https://bit.ly/3tPsMpV>.

I. INTRODUCTION

Robot manipulation for rigid-body objects has achieved significant progress in recent years, including grasping novel objects in clutter [22, 23], pushing novel objects [14], and solving Rubik’s cube [1]. Nevertheless, many daily objects we interact with are non-rigid, from folding clothes to packing grocery bags. Extending existing rigid-body object manipulation algorithms to deformable objects remains challenging because: 1) the degree of freedom of a deformable object is too large for traditional models, making explicit planning very difficult; 2) the dynamics of deformable objects are highly complex and non-linear due to the microscopic interactions in the object itself, which is difficult to model and leads to unpredictable behaviors [44]; 3) the deformation of an object leads to partial observability. Consider the example of flattening a cloth in Fig. 1: it is unclear how to mathematically specify the state of the cloth, and predicting the exact motion of the cloth is difficult even for a human, given the self-occlusion.

Pioneering works for deformable object manipulation rely on the low-dimensional geometric features to specify the object states and perform decision making by planning with a predefined dynamic model [40, 36, 25]. However, handcrafted geometric features often generalize poorly to unseen configurations, and predefined dynamics introduce accumulative error during long-horizon planning [9, 20]. With the recent advances

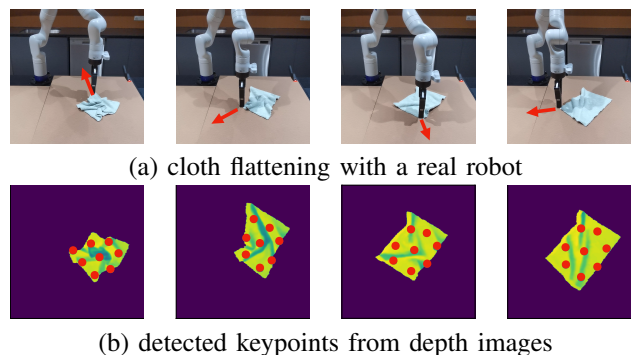


Fig. 1. Robot cloth flattening. (a) G-DOOM flattens a piece of crumpled cloth by reasoning a dynamic model learned from simulation data. (b) G-DOOM approximates the cloth, which has a large degree of freedom, by a low-dimensional keypoint-based graph generated from unsupervised learning.

in model-free visual policy learning [26, 27, 32], learning-based methods improve the deformable object manipulation performance. They avoid modeling the object state by directly mapping raw visual inputs to robot actions [24, 44, 38]. In particular, Yan et al. [46] introduces Contrastive Forward Models (CFMs) that learn a latent dynamic model from visual inputs and improve the sample efficiency of learning-based algorithms by explicit reasoning. Nevertheless, the geometric structures, which are essential to understanding the dynamics of a deformable object [16], have been neglected.

We argue that understanding the geometric structure of a deformable object is useful, but accurately modeling the dynamics of the entire deformable object is unnecessary for a manipulation task. Consider how a human manipulates a deformable object: to fold a piece of cloth, instead of considering the dynamics of the entire object, human only considers keypoints of the cloth, e.g., the collar, shoulders, and sleeves. However, detecting the keypoints and modeling their non-linear spatio-temporal interactions remain non-trivial.

We present *latent Graph dynamics for DefOrmable Object Manipulation* (G-DOOM), a framework for keypoint-based deformable object manipulation with only visual observations. Instead of explicitly modeling the entire object, G-DOOM abstracts the state of a deformable object as a low-dimensional keypoint-based graph with learned latent features. G-DOOM models the complex non-linear keypoint interactions by *Graph Neural Networks* (GNNs) directly learned from data. Such a formulation explicitly represents the state of the object, simplifies the non-linear dynamics, and avoids accumulative

errors of hand-crafted models. Specifically, G-DOOM discovers salient keypoints in an unsupervised manner from depth images with Transporter Networks [13] and extracts keypoint-centric feature vectors by masking the features with keypoint-based attention maps. The observed keypoints are grouped into a graph and high-level interactions among keypoints are effectively captured by Graph Neural Networks (GNNs). Nevertheless, abstraction into keypoints unavoidably leads to information loss. Moreover, the deformation of the object leads to self-occlusion and inaccurate keypoint detections, which eventually introduce partial observability to the task. To tackle these issues, we introduce a hybrid-scheme, *Recurrent Graph Dynamics*. It tracks the *belief*, i.e., the sufficient global statistics of the deformable object, with a Recurrent Neural Network (RNN), and predicts the next belief conditioned on the current belief and current graph state. By combining graph-based modeling with belief tracking, G-DOOM can successfully estimate a global state of a deformable object. Contrastive learning is further used to obtain a robust latent space that is accurate for planning. For effective decision making, we reason the learned dynamic model with a graph-based Model-Predictive Control (MPC), which bootstraps the search with the keypoint positions.

We evaluate G-DOOM on three deformable manipulation tasks: rope straightening, cloth flattening, and cloth folding. We first show that in a realistic simulator, NVidiaFlex [5], G-DOOM outperforms the state-of-the-art model-based deformable object manipulation methods on all three tasks. Besides, we show that our learned dynamic model using simulated data successfully transfers to a real-world scenario with a Kinova Gen3 robot.

II. RELATED WORKS

A. Deformable Object Manipulation

Deformable object manipulation is of significant importance to the robotics community, from the surgical robots [28, 10] to industrial manipulation [37]. Early works focus on identifying the object configuration with handcrafted visual features. The features are used to either index a set of pre-programmed trajectories or perform motion planning with a known mathematical dynamic model [45, 15, 39]. However, the hand-crafted model and the large degree of freedom of a deformable object make accurate reasoning difficult.

In contrast, model-free reinforcement learning (RL) maps the raw observations directly to a policy and avoids modeling the complex dynamics of a deformable object [26, 27, 29, 24, 44]. Despite its simplicity, the model-free policy is notorious for sample inefficiency and limited generalization. Model-based methods [19, 46] improve the sample efficiency by learning a dynamic model from visual inputs with vectors as the states and connect it with a motion planner. Using the vectors potentially loses the structural information of a deformable object. Our proposed G-DOOM benefits from both the sample efficiency of the model-based methods and the generality of the structural prior from keypoint-based representation.

B. Structured Dynamic Models

Recent advances on introducing the structural prior as an inductive bias to model structured environments or multi-agent systems have made great strides in improving the predictive quality of learned dynamic models [43, 16, 12, 13, 17]. Graph neural networks [11, 42, 47] are generally introduced to model the spatial interaction between objects, where each object is denoted as a node in the graph and the edges represent the spatial relationships between nodes. Unsupervised object-of-interest detection has been used to initialize the graph nodes, which is then connected to an action-conditioned transition model [43, 13, 17]. However, these methods use simple graph convolutions and transition networks, which is insufficient to tackle the complex keypoint interaction and partial observations of a deformable object. In contrast, G-DOOM adopts powerful Transformer-based Graph Convolution (TGConv) [47] composed with a RNN for belief tracking.

C. Contrastive Learning

Contrastive learning has been widely adopted in learning latent representations with various applications, e.g., machine translation [2], image representation learning [30, 4], pedestrian re-identification [35], and etc. The main idea is to maximize the correspondence of related data pairs (positive samples) and minimize the correspondence of irrelevant pairs (negative samples). In particular, the contrastive-learned dynamic models are more robust to the complicated observations, such as varying background and high-dimensional state-space [19, 46]. In particular, Yan et al. [46] introduces *Contrastive Forward Model* (CFM) that learns a latent dynamic model for a deformable object by standard InfoNCE loss [30]. We observe that given the partial observability and complex dynamics of a deformable object, which leads to sharp visual variations, the hinge contrastive loss used in G-DOOM gives a better-learned representation and improves the overall performance.

III. G-DOOM

A. Overview

We introduce *latent Graph Dynamics for DefOrmable Object Manipulation* (G-DOOM). (Fig. 2).

In contrast to standard latent models which represent the state with a single vector [7, 46, 19], G-DOOM abstracts a deformable object as a set of keypoints grouped into a graph G_t with learned node features, which provides rich semantics including keypoint positions, depths, textures, etc. However, modeling the high-level keypoint interactions is non-trivial. Consider manipulating a straightened rope: if we pull one end towards the other end, the rope loosens and the other end remains at its original position; if we drag one end towards the opposite direction, the rope remains straightened and both ends move together. This makes manually constructing a dynamic model of the keypoint-based representation difficult. We parameterize the interactions as attention-based Graph Neural Networks (GNNs) learned directly from data, which avoids manually constructing the model and improves the predictive accuracy. In addition, to tackle the partial observability caused

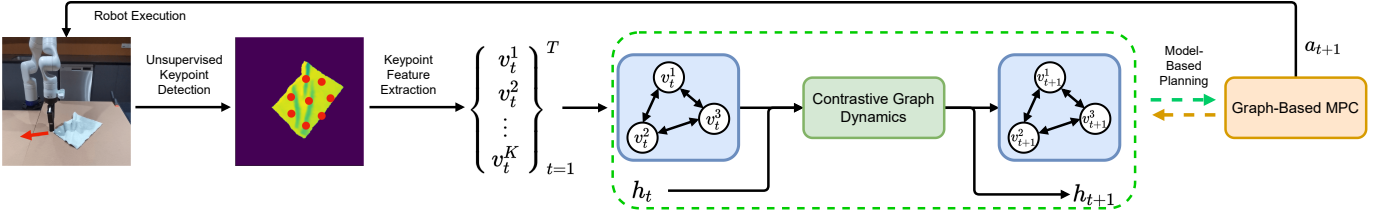


Fig. 2. G-DOOM Pipeline. G-DOOM performs unsupervised keypoint detection using depth images and extracts corresponding keypoint features $\{v_t^i\}_{i=1}^K$, which are composed into a graph according to the spatial relationships. Recurrent graph dynamics learns to predict the future states considering the spatio-temporal interaction among the local graph features $\{v_t^i\}_{i=1}^K$ and global statistics h_t , i.e., the belief. A graph-based Model-Predictive Control (MPC) reasons the learned graph dynamics and compute the action a_t conditioned on the detected keypoints.

by self-occlusion and inaccurate keypoint detection, G-DOOM adopts a hybrid approach, *Recurrent Graph Dynamics*. Besides the graph state G_t , it introduces an additional *belief* state, h_t , which tracks the sufficient statistics of an object by summarizing the graph states history G_1, G_2, \dots, G_t . The graph state update is then conditioned on the belief. The hybrid state representation performs implicit belief tracking and provides a global understanding during spatial interaction. For decision making, a simple yet effective graph-based MPC is used, which initializes the search based on the detected keypoints positions to improve the sample efficiency and convergence.

B. Unsupervised Keypoint Feature Learning

The key idea of G-DOOM is to down-sample a complex deformable object with a large degree of freedom as a low-dimensional graph. Since manually defining keypoints generalizes poorly to unseen configurations and objects, we discover the keypoints using offline unsupervised learning. In G-DOOM, we leverage the Transporter Networks [13] for keypoint detection and feature extraction.

The intuition of Transporter Networks is that the salient keypoints should contain sufficient information for reconstructing an image. Specifically, a Transporter Network consists of two major components, feature extractor f_{enc} and keypoint detector f_{kp} . For an image I , the feature extractor outputs a feature map $f_{enc}(I) \in \mathbb{R}^{H' \times W' \times C'}$ and the keypoint detector outputs a set of keypoints $f_{kp}(I) \in \mathbb{R}^{K \times 2}$, where H', W', C' are the height, width and channel number of the output feature map, and K is the number of keypoints. During training, a source image I_s and a target image I_t are sampled, and passed through f_{enc} and f_{kp} for feature extraction and keypoint detection. Next, a *transported* feature map is generated by composing the target features $f_{enc}(I_t)$ around the target keypoints $f_{kp}(I_t)$ with the background of the source feature map $f_{enc}(I_s)$

$$\begin{aligned} \text{Trans}(I_s, I_t) &= (1 - \mathcal{H}_{f_{kp}(I_s)})(1 - \mathcal{H}_{f_{kp}(I_t)})f_{enc}(I_s) \\ &\quad + \mathcal{H}_{f_{kp}(I_t)}f_{enc}(I_t) \end{aligned} \quad (1)$$

where $\mathcal{H}_{f_{kp}(I)} \in \mathbb{R}^{H' \times W' \times K}$ denotes the heatmap image with fixed-variance isotropic Gaussians around each keypoints in $f_{kp}(I)$. A decoding network f_{dec} then output a reconstruction of the target image $f_{dec}(\text{Trans}(I_s, I_t))$ and minimizes the reconstruction loss. This encourages the network to detect

keypoints that contain a sufficient amount of information to reconstruct the target image by composing the target image keypoint features with the background features of the source image. We pretrain and detach the Transporter networks from the rest of the pipeline because of the high GPU memory cost of end-to-end training.

The feature vector v^i of the i -th keypoint can be acquired by treating the keypoint heatmap as an attention mask over the feature space, then average over the channels with size C' .

$$v^i = 1/C' \sum_{i=1}^{C'} \mathcal{H}_{f_{kp}(I)}^i f_{enc}(I) \quad (2)$$

For a clean notation, we rewrite the corresponding keypoint position of the feature vector v^i as p^i . With depth images as the input, the node feature v^i learns to extract the depth, texture, and geometric information around position p^i , which provides rich statistics keypoint interaction modeling.

C. Recurrent Graph Dynamics

Given an observation I_t , we pass it to the Transporter, which gives the keypoint positions $P_t = \{p_t^i = (x_t^i, y_t^i)\}_{i=1}^K$ in the image space, and corresponding feature vectors $V_t = \{v_t^i\}_{i=1}^K$. We construct a graph state $G_t = (V_t, E_t)$, where edges $E_t = \{i, j\} \mid \|p_t^i - p_t^j\|_2 < \delta\}$ and δ is a hyper-parameter.

The spatial interactions among G_t are captured by graph neural networks. A standard graph neural network takes as input a graph $G_t = (V_t, E_t)$, and updates the node feature v_t^i by passing *messages* from the connected neighbors, i.e., $v_t^i = f_{gnn}(v_t^i, \{v_t^j\}_{j \in Nb(i)})$, where $Nb(i)$ denotes the neighbors of node i . For example, a basic Graph Convolutional Network (GCN)s [11] could be written as: $f_{gcn}(v_t^i, \{v_t^j\}_{j \in Nb(i)}) = \sum_{j \in Nb(i)} \eta \theta^j v_t^j$, where η is a normalizing constant. Intuitively, a GCN updates the node features by aggregating neighbor features with a transformation, and weighs nodes equally. However, standard GNNs are insufficient to model complex spatial keypoint interactions. To tackle this issue, we use a TGConv [47], which borrows the self-attention mechanism from the well-known Transformer Networks [41]. To address the partial observability and inaccurate keypoint detections, we propose to perform belief tracking with a Recurrent Neural Network along with the graphs, which conditions the spatial interaction modeling on a global state of the object.

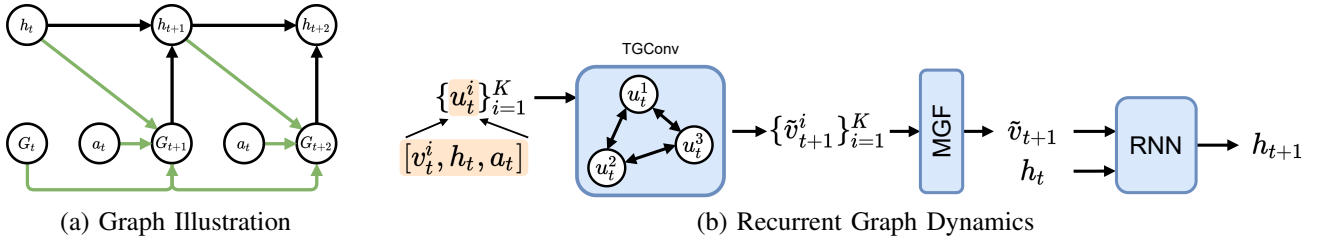


Fig. 3. (a) The graph illustration of recurrent graph dynamics (green arrow: graph update; black arrow: belief update). (b) Recurrent graph dynamics updates the node features by applying a Transformer-based Graph Convolution [47] over the concatenation of graph state features $\{v_t^i\}_{i=1}^K$, a belief h_t , and an action a_t . Given updated node features $\{\tilde{v}_{t+1}^i\}_{i=1}^K$, a global approximation \tilde{v}_{t+1} is extracted by applying Moment Generating Function (MGF) Features [19] and used to update the global belief h_{t+1} with a Recurrent Neural Network (RNN).

1) *Spatial Modeling with GNNs*: We argue that it is important to assign different weights to nodes during each message passing: nodes that are spatially closer to each other might have more influence than the nodes that are spatially far away. Specifically, we borrow the idea from *Transformer-based Graph Convolution* (TGConv) [47], which computes the message between nodes using the attention mechanism from Transformer Networks [41] by

$$\begin{aligned}
 v^i &= \text{LayerNorm} [f_{out}(\text{Attn}(i)) + v^i] \\
 \text{Attn}(i) &= \frac{\text{Softmax} \left(\left[\{m_t^{j \rightarrow i}\}_{j \in \text{Nb}(i) \cup \{i\}} \right] \right)}{\sqrt{d_k}} [\{v^j\}_{j \in \text{Nb}(i) \cup \{i\}}]^\top \\
 m_t^{j \rightarrow i} &= f_q(v^j)^\top f_k(v^i)
 \end{aligned} \quad (3)$$

where $\text{Nb}(i)$ denotes the indices of the neighbors of node i in graph G_t , f_q , f_k , and f_{out} are fully connected layers for computing the query vector, key vector and output vector, d_k is the dimension of the key vector, and $[\{x_i\}_{i=1}^n]$ is the concatenation of n vectors. For a simple notation, we rewrite the above process as $v^i = \text{TGConv}(v^i, \{v^j\}_{j=1}^K)$.

For simplicity, we assume G_t is a fully connected graph, which is valid given a relatively small deformable object. A more complex formulation such as causal inference could be considered [17], and we leave it for future study. Empirically, we find that TGConv gives the best-learned dynamics.

2) *Graph Belief Tracking*: However, the visual observation of a deformable object is partially observable due to the self-occlusion, and the unsupervised keypoint detection might produce inconsistent and inaccurate keypoint detections. To tackle these issues, we propose to combine the graph convolutions with a Recurrent Neural Network (RNN) to track the belief by a belief state h_t . Ideally, h_t summarizes the history of the graph states G_1, G_t, \dots, G_t and estimates a global state of the object given past partial observations.

We implement the graph-based belief tracking as follows:

$$\tilde{v}_{t+1}^i = \text{TGConv}([v_t^i, h_t, a_t], \{[v_t^i, h_t, a_t]\}_{i=1}^K) \quad (4)$$

$$h_{t+1} = \text{RNN}(h_t, \{\tilde{v}_{t+1}^i\}_{i=1}^K) \quad (5)$$

where Eqn. 4 updates the observed graph node features $\{v_t^i\}_{i=1}^K$ conditioned on the action a_t and belief h_t , and Eqn. 5 updates the belief h_t with the predicted node features $\{\tilde{v}_{t+1}^i\}_{i=1}^K$. Hence, h_t provides a global understanding to the the spatial modeling.

Node features set $\{\tilde{v}_{t+1}^i\}_{i=1}^K$ cannot be used as input to a RNN directly, and we aim to extract a single-vector approximation, \tilde{v}_{t+1} to the set. One of the standard set feature aggregation method is to treat the set as a sequence, and aggregate the set features with a separate RNN [8], which, nonetheless, ignores the permutation invariance of the set and complicate the optimization landscape due to the recurrence [21]. Alternatively, global-max pooling and mean-pooling are widely-adopted in point-cloud literature [33, 34, 48, 47]. Nevertheless, the fixed operation loses the statistical correctness of a distribution. In G-DOOM, we use the Moment-Generating Function Features (MGFs) [21] to merge the keypoints. By considering the keypoints as an empirical distribution specification of an object, the MGF of an object is statistically an alternative specification to the object [3]. We derive \tilde{v}_{t+1} as

$$\tilde{v}_t = \text{MGF}(\{v_t^i\}_{i=1}^K) = \left[\frac{1}{K} \sum_{i=1}^K v_t^i, \sum_{i=1}^K e^{\theta^\top v_t^i} \right] \quad (6)$$

where θ is a learnable matrix. Intuitively, \tilde{v}_t contains the first-order moment, i.e., the mean $\frac{1}{K} \sum_{i=1}^K v_t^i$, and a set of high-order moments $\sum_{i=1}^K e^{\theta^\top v_t^i}$ learned from data. More details about MGF features are available in the appendix.

Eventually, we rewrite the belief update in Eqn. 5 by

$$h_{t+1} = \text{RNN}(h_t, \tilde{v}_t) \quad (7)$$

D. Contrastive Dynamics Learning

Contrastive learning has been widely adopted in representation learning with various applications. In the context of learning dynamic models, it generally improves the robustness of the model against noisy and complex observations [12, 21, 46]. The key idea is to minimize the difference between a true encoding-prediction pair (v_t, \tilde{v}_t) , while maximizing the difference between the prediction and a set of irrelevant encodings $\{v_n\}_{n=1}^N$. This produces a latent space where predictions are well-separated from incorrect encodings.

Given the observation sequence $I_{1:t}$, we unroll the model for $T - t$ steps, predict the graph sequence $\{\tilde{v}_{t+1:T}^i\}_{i=1}^K$ using Eqn. 7 and minimize the distance between the predicted graphs and the encoded graphs $\{v_{t+1:T}^i\}_{i=1}^K$ from the future observations $I_{t+1:T}$. To avoid exact graph matching, we instead minimize the distance between the single-vector representations $\tilde{v}_t = \text{MGF}(\{\tilde{v}_t^i\}_{i=1}^K)$ and $v_t = \text{MGF}(\{v_t^i\}_{i=1}^K)$. We adopt a

contrastive objective L_D for dynamics:

$$L_D = \sum_{t'=t+1}^T \left[\|\tilde{v}_{t'} - v_{t'}\|_2 + \sum_{n=1}^N \max(0, \gamma - \|\tilde{v}_{t'} - v_n\|_2) \right] \quad (8)$$

where $\{v_n\}_{n=1}^N$ are negative states encoded from a set of observations $\{I_n\}_{n=1}^N$ sampled randomly from the datasets. Specifically, we adopt an energy-based hinge-loss to improve the robustness of the loss function against outliers [12], where γ is a hyper-parameter. We find $\gamma = 1$ to be a good choice.

To allow planning with the learned dynamics, we predict a state-dependent the reward by $\tilde{r}_t = f_r(\tilde{v}_t)$. We train the reward predictor by $L_R = \sum_{t'=t+1}^T (\tilde{r}_{t'} - r_{t'})^2$. Thus, to optimize the dynamics of G-DOOM, the overall training loss is given by

$$L = L_D + \alpha L_R \quad (9)$$

where α is a hyper-parameter that balances two training objectives and we find $\alpha = 1$ works well in practice.

G-DOOM is also capable of goal-oriented manipulation. Given a goal image I_g , G-DOOM extracts the keypoint features $\{v_g^i\}_{i=1}^K$ and construct the MGF feature $\bar{v}_g = \text{MGF}(\{v_g^i\}_{i=1}^K)$. The reward is defined as $r_g = -\|\bar{v} - \bar{v}_g\|_2$, where \bar{v} is the MGF feature of the current state. However, we found such an objective less informative, because a top-down 2D image provides no 3D information about the object. We focus on reward function learning and present additional goal-oriented manipulation results in the appendix.

E. Graph-Based Model-Predictive Control

Throughout our tasks, we use a pick-and-place action, $a = [x_s, y_s, x_g, y_g]$, where (x_s, y_s) is the pick position and (x_g, y_g) is the place position. Given the learned dynamic model, standard planning algorithms can be used to determine the action by searching with an initial action distribution $a_0 \sim \mathcal{N}(\mu_0, \sigma_0)$, where $\mu_0 = [x_0, y_0, x_0, y_0]$. Normally, $x_0 = y_0 = 0$ and $\sigma = \mathbb{I}$. Inspired by the human cloth folding, we observe that an effective action normally takes effect around the keypoints. Thus, we develop a simple yet effective graph-based cross entropy method for planning.

The intuition behind graph-based MPC is that we solve K separate MPC problems around each of the K keypoints, $\{p^i = (x^i, y^i)\}_{i=1}^K$. For process i , we initialize the search action $a^i = [x^i, y^i, x^i, y^i]$. After the planning finished, we obtain K separate (a^{i*}, \tilde{R}^{i*}) pairs, where a^{i*} is the output action of the MPC process centered at keypoint p^i , and \tilde{R}^{i*} is the corresponding predicted accumulative reward using the learned dynamics and reward model. At last, the final action is chosen according to $a^* = \arg \max_{a^{i*}} \tilde{R}^{i*}$.

To solve the MPC, we use a simple Cross-Entropy Method (CEM). Note that given the learned latent graphs, we could also define the reward as the difference between the learned latent states and the goal state, which would allow us to perform goal-based manipulation similar to Yan et al. [46]. We leave that approach for future study. A detailed description of the algorithm is available in the appendix.

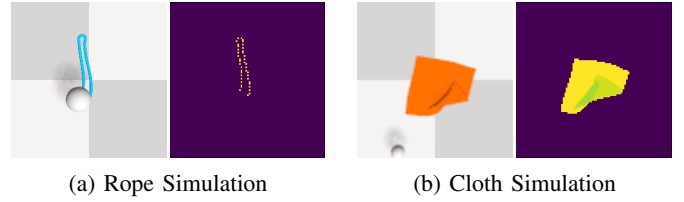


Fig. 4. We use a high-fidelity particle-based simulator, NVidia-Flex [5] in our experiment. Specifically, we use depth images as the input to our network to minimize the sim-to-real gap.

IV. EXPERIMENTS

We first evaluate the proposed G-DOOM on a set of rope straightening and cloth manipulation tasks in a high-fidelity simulator, NVidia-Flex [5]. To minimize the sim-to-real gap, we use masked depth images as the input, and we show that our learned dynamic model transfers directly to a real-robot.

We compare G-DOOM with the state-of-the-art (SOTA) model-based deformable object manipulation method, *Contrastive Forward Model* (CFM) [46], and a SOTA general-purpose model-based RL method, PlaNet [7]. For all baselines, we use the publicly available implementations. For a fair comparison, we adapt the original goal-oriented CFM to reward-driven by adding an additional reward predictor. We show that: 1) G-DOOM generally outperforms all baselines in all tasks; 2) the recurrent graph dynamics improves the quality of the learned dynamics; 3) contrastive learning improves the accuracy of learned dynamics; 4) graph-based MPC generally improves overall performance.

A. Experiment Setup

1) *Simulation Environment*: We build our simulator upon SoftGym [18], a soft-body simulator based on NVidia-Flex [5], the state-of-the-art (SOTA) particle-based simulator that simulates objects as a set of particles. Example images are shown in Fig. 4. We make certain modifications on SoftGym to better match the real-robot scenarios, where we have:

- *Observation space*. The observation is a depth image of size 96×96 with depth values, indicating the distance to a top-down simulated camera. Specifically, we perform object segmentation and set the background value to 0.
- *Action space*. As mentioned in Sect. III-E, we use a pick-and-place action, $a_t = [x_s, y_s, x_g, y_g]$, where (x_s, y_s) is the pick position and (x_g, y_g) is the place position. Action size greater than 25% of the state space will be clipped, i.e., given the image of size 96 and $a_t = (x_s, y_s, x_g, y_g)$, $\|(x_s - x_g, y_s - y_g)\|_2 < 24$.

2) *Tasks*: We evaluate the proposed G-DOOM on 2 cloth manipulation and 4 rope straightening tasks.

- *Rope Straightening*. The task is to straighten a rope and position it at the center of the image with different orientations ($0^\circ, 45^\circ, 90^\circ, 135^\circ$). The challenge is to understand the complex non-linear dynamics of a deformable object. We define the reward as $r = -\|p_c - p_g\|_2$, where p_c, p_g are the current and goal positions of the two end points.
- *Cloth Manipulation*. The cloth manipulation tasks are more challenging than the rope straightening because

TABLE I
SIMULATION EXPERIMENT: SUCCESS RATE (%)

	Rope				Cloth	
	0°	45°	90°	135°	Flatten	Fold
CFM	24.7	18.4	9.1	11.6	29.2	59.6
PlaNet	39.1	68.1	64.4	82.4	35.9	73.2
G-DOOM	65.7	80.3	73.2	98.1	95.1	92.5

TABLE II
SIMULATION EXPERIMENT: DYNAMICS ACCURACY 1@50 (%)

	Rope				Cloth	
	0°	45°	90°	135°	Flatten	Fold
CFM	47.7	44.8	48.4	49.6	59.4	61.1
PlaNet	-	-	-	-	-	-
G-DOOM	99.9	99.9	99.8	99.9	99.9	99.9

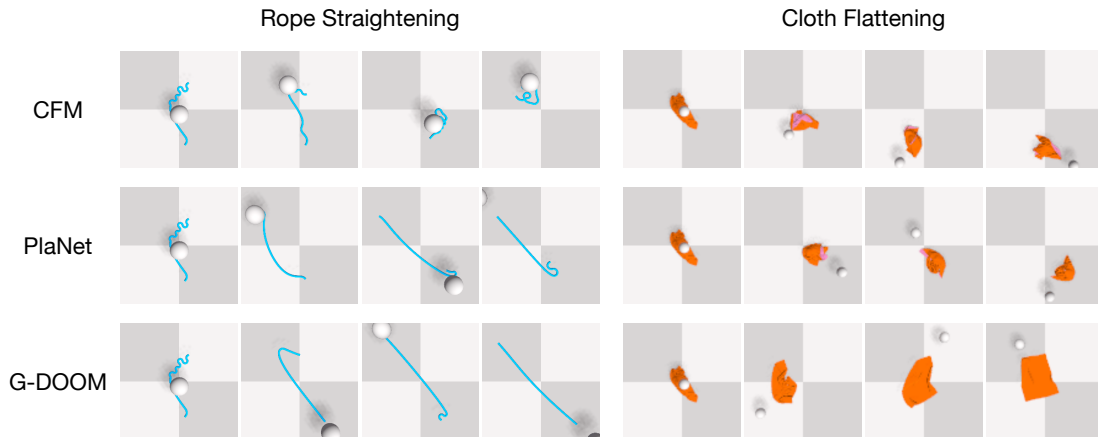


Fig. 5. Visualizations of execution trajectories in the simulator (Rope Straightening 135° and Cloth Flattening). Note that in the rope straightening task, G-DOOM reached the goal within 3 steps so we repeated the visualization of the last two frames.

of the partial observability caused by self-occlusions. It consists of two sub-tasks: 1) cloth flattening, where the task is to flatten a piece of randomly crumpled cloth. The reward r is defined as the area covered by the cloth; 2) cloth folding, where the task is to fold a piece of randomly positioned flattened cloth in half. The reward is defined as the $r = -\|p_l - p_r\|_2 - 1.2 * \|p_l - p_l^0\|$, where p_l, p_r, p_l^0 are the particle positions of the left half, right half and the initial position of the left half.

3) *Data Collection*: For each task, we collect 5000 trajectories of length 20 using random actions, with 1000 randomly generated the initial configuration of the object, where the size of the cloth and the length of the rope are randomized.

4) *Model Learning*: We split the training of G-DOOM into two phases. In the first phase, we pre-train the Transporter network. Qualitatively, we find using $K = 8$ keypoints for cloth manipulation and $K = 3$ keypoints for rope straightening performs well in practice. Next, we freeze the weights of the Transporter and train the dynamic model. For a fair comparison, we train all baselines with the same number of epochs. All our models are trained with NVidia RTX 2080Ti GPUs. A detailed training scheme is available in the appendix.

5) *Evaluation Setups*: In all tasks, we allow a maximum sequence length of 20 steps and report the success rate over 1000 different random seeds. We define the success criteria as the distance to goal given the ground-truth particle locations in the simulator. For the *contrastive learning methods* (G-DOOM and CFM), we also report the top 1 prediction accuracy. This is measured by unrolling the dynamic model for 20 steps, and measure the prediction error $d(\tilde{s}_t, s_t)$ between

the predicted state \tilde{s}_t and the encoded state s_t , against N negative samples $\{s^j\}_{j=1}^J$. The top 1 accuracy is measured by $Acc = 1/N \sum_{n=1}^N \mathbb{I}(\forall j, d(\tilde{s}_t^n, s_t^n) < d(\tilde{s}_t^n, s_j^n))$, which means the prediction error should be smaller than the distance to all 50 negative samples. This metric measures the quality of a contrastive-learned dynamic model [12]. Detailed setups and the reward achieved are in the appendix.

B. Simulation Experiment

We present the highest reward achieved in Tab. I and the dynamics accuracy for in Tab. II. We observe that:

Graph-based dynamics better captures complex dynamics. In 5 out of 6 cases, the proposed G-DOOM achieves the highest success rate, and it performs comparably with PlaNet on the other one. It suggests that the graph-based dynamics generally improve the quality of the learned dynamic model and the overall performance, compared to the single-vector-based dynamics. Besides, in rope straightening tasks, where the dynamics are relatively simple, PlaNet achieves reasonably good performance compared with G-DOOM. However, on cloth manipulation, where more complex dynamics and partial observability are introduced, G-DOOM outperforms both PlaNet and CFM. This further emphasizes the benefit of graph structure in the dynamic model.

Belief tracking is necessary for complex dynamics. Both PlaNet and G-DOOM perform belief tracking with an additional hidden vector using RNNs, while CFM is state-dependent, i.e., remembers no history. In most of the cases, CFM performs worse than PlaNet and G-DOOM, which is contradictory to the original results of the CFM paper [46]. The reason is

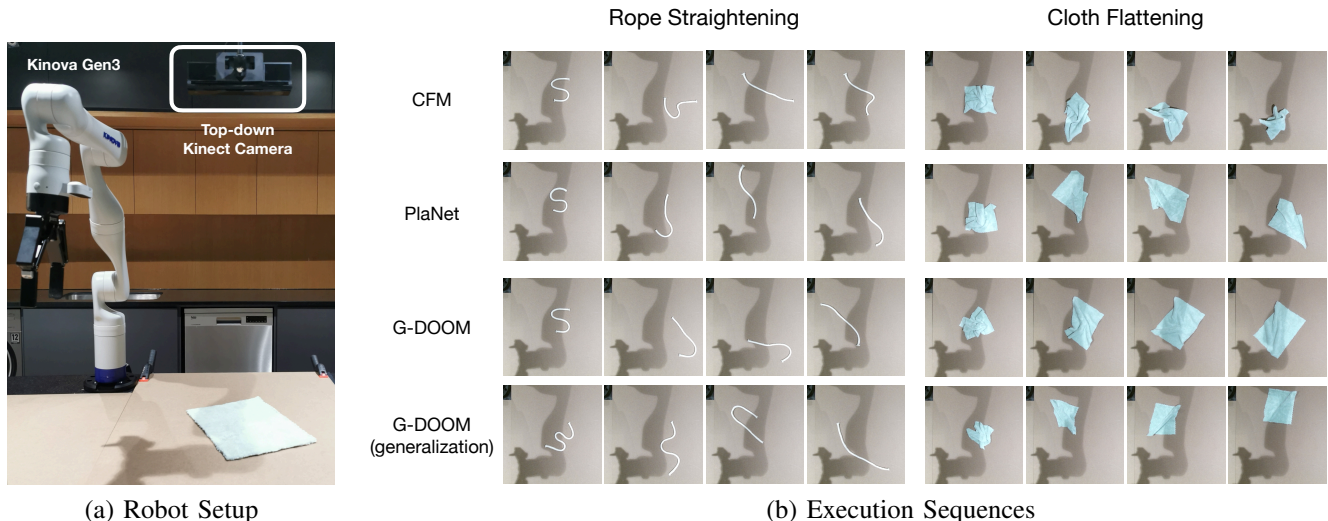


Fig. 6. (a) We use a Kinova Gen3 robot with a Robotiq gripper for the experiment. A top-down Kinect 2.0 camera is used to produce depth images. (b) Visualizations of execution trajectories on a real robot (Rope Straightening 135° and Cloth Flattening). G-DOOM (generalization) shows that our trained model generalizes to different objects with different initial configurations, e.g., longer ropes and smaller cloths.

potentially that originally, CFM allows a longer execution sequence length with a smaller step size: 40 steps are allowed for rope straightening and 100 steps are allowed for cloth manipulation. However, in our case, a larger step size is used with a much shorter time limit: 20 steps for all tasks, which leads to more complex dynamics. Besides, the masked depth images contain fewer signals (most of the pixels are 0), which makes it difficult for pure contrastive learning methods.

G-DOOM learns a more robust contrastive dynamic model. In Tab. II, CFM achieves a relatively low top 1 dynamics accuracy, while G-DOOM achieves almost 100% accuracy. This explains the low success rate of CFM. G-DOOM focuses on keypoints with rich features and learns a better dynamic model with the recurrent graph dynamics.

Example visualizations are in Fig. 5. Both PlaNet and G-DOOM successfully straighten the rope with desired orientation, while CFM failed. For cloth flattening, both PlaNet and CFM struggle, but G-DOOM gives a high success rate.

C. Real Robot Experiment

We further evaluate our learned model on a Kinova Gen3 robot, as shown in Fig. 6.a. To collect high-quality depth images, we mount a top-down Kinect 2.0 camera over the workspace. We observe that high-quality depth images and the simplified pick-and-place action model help to minimize the sim-to-real gap, and our trained models transfer directly to the real robot. Detailed robot setups are provided in the appendix.

Evaluation metric: We measure the distance-to-goal by counting the number of pixels within a goal region. Denoting the set of pixels covered by a deformable object as S_o , we define the score as follows. For rope straightening tasks, we define goal region S_g to be a rectangle centered in the middle of the image rotated for different degrees (0° , 45° , 90° , 135°), and measure score = $|S_o \cap S_g|$; for cloth flattening, we simply compute the total number of pixels of the covered area by score = $|S_o|$; for cloth folding, we define the goal area to be half of the cloth

TABLE III
REAL ROBOT EXPERIMENT RESULTS

	Rope				Cloth	
	0°	45°	90°	135°	Flatten	Fold
CFM	1.378	33.26	45.64	14.49	515.24	-158.15
PlaNet	40.93	68.52	36.92	11.51	946.82	-199.08
G-DOOM	81.91	67.56	47.92	53.50	1,458.15	-42.15

in the initial frame and measure score = $-||S_o| - |S_g||$. All results are averaged over 3 random seeds.

Results: The quantitative results of the real robot experiments are given in Tab. III and visualizations are provided in Fig. 6.

G-DOOM generally outperforms the baselines. In real robot experiments, G-DOOM achieves higher scores than the baselines, which is consistent with our simulation results.

Graph-based dynamics allow G-DOOM to generalize better. In the simulation, PlaNet achieves reasonable performance on rope straightening tasks, while on a real robot, it fails on rope straightening 0° and 135° . In contrast, G-DOOM generalizes in all cases. This is potentially because by down-sampling an object into a keypoint-based graph, G-DOOM constructs an information bottleneck that filters the high-frequency noise and maintains a minimum amount of information for modeling the dynamics. Also, the recurrent graph dynamics compensate for the information loss. As shown in Fig.6 G-DOOM (generalization), our trained model can be directly applied to different objects, e.g., longer ropes and smaller cloths.

Due to the space limit, we visualize only two real robot tasks in Fig. 6.b. More visualizations are available in the appendix.

D. Ablation Studies

We conduct an extensive ablation study to understand the influence of each proposed G-DOOM component (Tab. IV).

Imposing a graph structure in the dynamic model generally improves the performance of the algorithm. Compared with the standard G-DOOM, the NoGraph variant removes the graph-

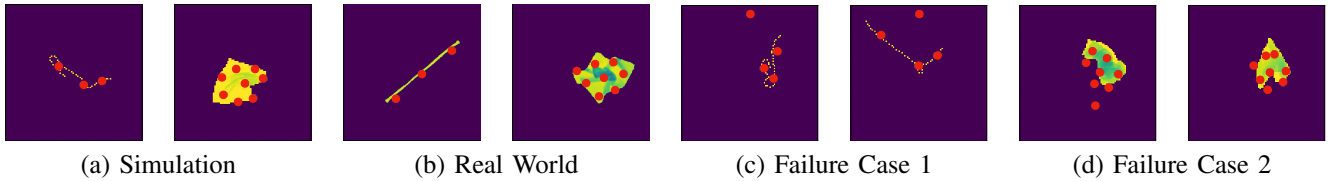


Fig. 7. Keypoint visualizations on depth images. The detected keypoints are salient and transfer from simulation environment to real-world observations. The keypoint detector might fail when incorrect number of keypoints is specified or the object is under extreme deformation.

based representation and dynamics. We observe that G-DOOM generally outperforms the NoGraph variant in all tasks, which suggests that the graph-based representation better captures the dynamics of a deformable object.

Belief tracking with RNN is necessary to handle partial observability. The NoRNN variant removes the RNN and directly uses a single TGConv as the transition function f_{gmn} . We observe that NoRNN achieves reasonable performance on rope straightening tasks, while on cloth manipulation where partial observability exists, its performance degrades. It suggests that belief-tracking with a RNN is useful to tackle the self-occlusions in cloth manipulation tasks.

Hinge-loss-based contrastive learning improves the robustness of the learned dynamic model. The NoContrastive variant of G-DOOM removes the contrastive component in loss function Eqn. 8 and minimizes only the difference between the true states and predicted states. Also, the InfoNCE variant replaces the hinge loss by the standard InfoNCE [30] used in CFM. They perform generally worse than G-DOOM, which suggests contrastive learning is necessary, and hinge loss improves the robustness of the model.

Graph-based CEM can improve the search performance. The CEM variant replaces the Graph-based CEM with a standard CEM, without using the keypoint positions as a prior to initialize the search. As a result, given the same number of optimization iterations, the standard CEM shows worse performance than the original G-DOOM.

TGConv improves the spatial modeling ability for a deformable object. The GAT variant of G-DOOM replaces the TGConv graph convolution by the widely adopted Graph Attention Networks (GAT) [42]. After replacing the TGConv with GAT, we observe that the overall performance of G-DOOM generally degrades, which is because that using the relatively simple GAT is insufficient to model the complex spatio-temporal microscopic interaction of a deformable object.

MGF features improves the global feature extraction of a graph. The MaxPool variant of G-DOOM replaces the MGF features for global feature extraction by the MaxPooling technique generally used in point cloud learning literature [33, 34]. G-DOOM with MGF features generally gives a higher success rate than the MaxPool variant.

E. Visualization of Keypoints

We visualize the learned keypoints in both simulation and real-robot setups. We observe that the keypoint detector outputs salient keypoints for both rope and cloth (Fig. 7.a). It also transfers directly to real-world depth images (Fig. 7.b). However, the failure cases arise under two conditions: (1) in

TABLE IV
ABLATION STUDY: SUCCESS RATE (%)

	Rope				Cloth	
	0°	45°	90°	135°	Flatten	Fold
NoGraph	7.2	5.7	4.1	34.4	75.8	64.1
NoRNN	34.1	37.7	69.3	84.1	78.7	22.9
NoContrastive	0.2	0.7	3.8	5.5	29.7	29.7
InfoNCE	3.5	69.4	26.8	9.2	31.0	61.9
CEM	25.0	72.0	39.0	33.6	91.9	58.5
GAT	13.2	9.4	28.3	31.7	37.7	28.3
MaxPool	28.1	31.9	29.9	65.5	94.8	55.7
G-DOOM	65.7	80.3	73.2	98.1	95.1	92.5

Fig. 7.c, when we train the keypoint detector with an improper number of keypoints (4 keypoints) on a rope manipulation task, one of the keypoints would lie outside the object. (2) since our training objective (Eqn. 1) encourages the keypoints to spread across the object, it occurs that when the cloth is under extreme deformation, e.g., crumpled into a small piece, some of the keypoint detections are inaccurate. The incorrect keypoints introduces noise feature and partial observability to the model, which potentially influences the overall performance of G-DOOM. This emphasizes the importance of the proposed recurrent graph dynamics, which improves the robustness of the model against both noise and partial observability. It also explains the failure of the ablation models: without a robust model, they are susceptible to noisy keypoint detections.

V. CONCLUSION

In this paper, we introduce G-DOOM, a graph-based approach for deformable object manipulation. We observe that modeling the full dynamics of a deformable object, which has a large degree of freedom, is unnecessary. G-DOOM performs unsupervised keypoint detection and feature extraction, model the spatio-temporal keypoint interactions using recurrent graph dynamics, and conducts model-based planning using the learned model. G-DOOM tackles the partial observability caused by the self-occlusion of deformable objects by belief tracking with a recurrent neural network. A graph-based MPC is introduced to improve the planning performance. We show that G-DOOM outperforms the SOTA deformable object manipulation methods in both simulation and a real robot.

However, the current paradigm only supports a fixed number of visually salient keypoints. The inaccurate detection introduces noise to the dynamic model. Future works could consider learning temporally and robust keypoints by jointly training the perception and the dynamics module, which might experience high GPU memory cost.

REFERENCES

- [1] Ilge Akkaya, Marcin Andrychowicz, Maciek Chociej, Mateusz Litwin, Bob McGrew, Arthur Petron, Alex Paino, Matthias Plappert, Glenn Powell, Raphael Ribas, et al. Solving rubik’s cube with a robot hand. *arXiv preprint arXiv:1910.07113*, 2019.
- [2] Antoine Bordes, Nicolas Usunier, Alberto García-Durán, Jason Weston, and Oksana Yakhnenko. Translating embeddings for modeling multi-relational data. In Christopher J. C. Burges, Léon Bottou, Zoubin Ghahramani, and Kilian Q. Weinberger, editors, *Advances in Neural Information Processing Systems*, pages 2787–2795, 2013.
- [3] Michael George Bulmer. *Principles of statistics*. Courier Corporation, 1979.
- [4] Ting Chen, Simon Kornblith, Mohammad Norouzi, and Geoffrey E. Hinton. A simple framework for contrastive learning of visual representations. In *Proceedings of the 37th International Conference on Machine Learning, ICML 2020, 13-18 July 2020, Virtual Event*, volume 119 of *Proceedings of Machine Learning Research*, pages 1597–1607. PMLR, 2020. URL <http://proceedings.mlr.press/v119/chen20j.html>.
- [5] Gianni Ciccarelli. Particle-based fluid simulation with nvidia flex. 2019.
- [6] Tuomas Haarnoja, Aurick Zhou, Pieter Abbeel, and Sergey Levine. Soft actor-critic: Off-policy maximum entropy deep reinforcement learning with a stochastic actor. In Jennifer G. Dy and Andreas Krause, editors, *Proceedings of the 35th International Conference on Machine Learning, ICML 2018, Stockholmsmässan, Stockholm, Sweden, July 10-15, 2018*, volume 80 of *Proceedings of Machine Learning Research*, pages 1856–1865. PMLR, 2018. URL <http://proceedings.mlr.press/v80/haarnoja18b.html>.
- [7] Danijar Hafner, Timothy P. Lillicrap, Ian Fischer, Ruben Villegas, David Ha, Honglak Lee, and James Davidson. Learning latent dynamics for planning from pixels. In Kamalika Chaudhuri and Ruslan Salakhutdinov, editors, *Proceedings of the 36th International Conference on Machine Learning, ICML 2019, 9-15 June 2019, Long Beach, California, USA*, volume 97 of *Proceedings of Machine Learning Research*, pages 2555–2565. PMLR, 2019. URL <http://proceedings.mlr.press/v97/hafner19a.html>.
- [8] Maximilian Igl, Luisa M. Zintgraf, Tuan Anh Le, Frank Wood, and Shimon Whiteson. Deep variational reinforcement learning for pomdps. In Jennifer G. Dy and Andreas Krause, editors, *Proceedings of the 35th International Conference on Machine Learning, ICML 2018, Stockholmsmässan, Stockholm, Sweden, July 10-15, 2018*, volume 80 of *Proceedings of Machine Learning Research*, pages 2122–2131. PMLR, 2018. URL <http://proceedings.mlr.press/v80/igl18a.html>.
- [9] Peter Karkus, Xiao Ma, David Hsu, Leslie Pack Kaelbling, Wee Sun Lee, and Tomás Lozano-Pérez. Differentiable algorithm networks for composable robot learning. *Robotics: Science and Systems*, 2019.
- [10] Martin Kibsgaard, Kasper K Thomsen, and Martin Kraus. Simulation of surgical cutting in deformable bodies using a game engine. In *2014 International Conference on Computer Graphics Theory and Applications (GRAPP)*, pages 1–6. IEEE, 2014.
- [11] Thomas N Kipf and Max Welling. Semi-supervised classification with graph convolutional networks. *arXiv preprint arXiv:1609.02907*, 2016.
- [12] Thomas N. Kipf, Elise van der Pol, and Max Welling. Contrastive learning of structured world models. In *8th International Conference on Learning Representations, ICLR 2020, Addis Ababa, Ethiopia, April 26-30, 2020*. OpenReview.net, 2020. URL <https://openreview.net/forum?id=H1gax6VtDB>.
- [13] Tejas D Kulkarni, Ankush Gupta, Catalin Ionescu, Sebastian Borgeaud, Malcolm Reynolds, Andrew Zisserman, and Volodymyr Mnih. Unsupervised learning of object keypoints for perception and control. *Advances in neural information processing systems*, 32:10724–10734, 2019.
- [14] Jue Kun Li, Wee Sun Lee, and David Hsu. Push-net: Deep planar pushing for objects with unknown physical properties. In *Robotics: Science and Systems*, volume 14, pages 1–9, 2018.
- [15] Yinxiao Li, Yonghao Yue, Danfei Xu, Eitan Grinspun, and Peter K Allen. Folding deformable objects using predictive simulation and trajectory optimization. In *2015 IEEE/RSJ International Conference on Intelligent Robots and Systems (IROS)*, pages 6000–6006. IEEE, 2015.
- [16] Yunzhu Li, Jiajun Wu, Russ Tedrake, Joshua B. Tenenbaum, and Antonio Torralba. Learning particle dynamics for manipulating rigid bodies, deformable objects, and fluids. In *7th International Conference on Learning Representations, ICLR 2019, New Orleans, LA, USA, May 6-9, 2019*. OpenReview.net, 2019. URL <https://openreview.net/forum?id=rJgbSn09Ym>.
- [17] Yunzhu Li, Antonio Torralba, Anima Anandkumar, Dieter Fox, and Animesh Garg. Causal discovery in physical systems from videos. *Advances in Neural Information Processing Systems*, 33, 2020.
- [18] Xingyu Lin, Yufei Wang, Jake Olkin, and David Held. Softgym: Benchmarking deep reinforcement learning for deformable object manipulation. *arXiv preprint arXiv:2011.07215*, 2020.
- [19] Xiao Ma, Siwei Chen, David Hsu, and Wee Sun Lee. Contrastive variational model-based reinforcement learning for complex observations. *arXiv preprint arXiv:2008.02430*, 2020.
- [20] Xiao Ma, Péter Karkus, David Hsu, and Wee Sun Lee. Particle filter recurrent neural networks. In *The Thirty-Fourth AAAI Conference on Artificial Intelligence, AAAI 2020*, pages 5101–5108. AAAI Press, 2020.
- [21] Xiao Ma, Péter Karkus, David Hsu, Wee Sun Lee, and Nan Ye. Discriminative particle filter reinforcement learning for complex partial observations. In *8th International Conference on Learning Representations, ICLR 2020, Addis Ababa, Ethiopia, April 26-30, 2020*.

- OpenReview.net, 2020.
- [22] Jeffrey Mahler, Florian T Pokorny, Brian Hou, Melrose Roderick, Michael Laskey, Mathieu Aubry, Kai Kohlhoff, Torsten Kröger, James Kuffner, and Ken Goldberg. Dex-net 1.0: A cloud-based network of 3d objects for robust grasp planning using a multi-armed bandit model with correlated rewards. In *2016 IEEE international conference on robotics and automation (ICRA)*, pages 1957–1964. IEEE, 2016.
- [23] Jeffrey Mahler, Jacky Liang, Sherdil Niyaz, Michael Laskey, Richard Doan, Xinyu Liu, Juan Aparicio Ojea, and Ken Goldberg. Dex-net 2.0: Deep learning to plan robust grasps with synthetic point clouds and analytic grasp metrics. In Nancy M. Amato, Siddhartha S. Srinivasa, Nora Ayanian, and Scott Kuindersma, editors, *Robotics: Science and Systems XIII, Massachusetts Institute of Technology, Cambridge, Massachusetts, USA, July 12-16, 2017*, 2017.
- [24] Jan Matas, Stephen James, and Andrew J Davison. Sim-to-real reinforcement learning for deformable object manipulation. In *Conference on Robot Learning*, pages 734–743. PMLR, 2018.
- [25] Stephen Miller, Jur Van Den Berg, Mario Fritz, Trevor Darrell, Ken Goldberg, and Pieter Abbeel. A geometric approach to robotic laundry folding. *The International Journal of Robotics Research*, 31(2):249–267, 2012.
- [26] Volodymyr Mnih, Koray Kavukcuoglu, David Silver, Alex Graves, Ioannis Antonoglou, Daan Wierstra, and Martin Riedmiller. Playing atari with deep reinforcement learning. *arXiv preprint arXiv:1312.5602*, 2013.
- [27] Volodymyr Mnih, Adrià Puigdomènech Badia, Mehdi Mirza, Alex Graves, Timothy P. Lillicrap, Tim Harley, David Silver, and Koray Kavukcuoglu. Asynchronous methods for deep reinforcement learning. In Maria-Florina Balcan and Kilian Q. Weinberger, editors, *Proceedings of the 33rd International Conference on Machine Learning, ICML, 2016*.
- [28] Peter Mountney, Benny Lo, Surapa Thiemjarus, Danail Stoyanov, and Guang Zhong-Yang. A probabilistic framework for tracking deformable soft tissue in minimally invasive surgery. In *International Conference on Medical Image Computing and Computer-Assisted Intervention*, pages 34–41. Springer, 2007.
- [29] Junhyuk Oh, Satinder Singh, and Honglak Lee. Value prediction network. In Isabelle Guyon, Ulrike von Luxburg, Samy Bengio, Hanna M. Wallach, Rob Fergus, S. V. N. Vishwanathan, and Roman Garnett, editors, *Advances in Neural Information Processing Systems*, 2017.
- [30] Aaron van den Oord, Yazhe Li, and Oriol Vinyals. Representation learning with contrastive predictive coding. *arXiv preprint arXiv:1807.03748*, 2018.
- [31] Adam Paszke, Sam Gross, Francisco Massa, Adam Lerer, James Bradbury, Gregory Chanan, Trevor Killeen, Zeming Lin, Natalia Gimelshein, Luca Antiga, Alban Desmaison, Andreas Kopf, Edward Yang, Zachary DeVito, Martin Rai-son, Alykhan Tejani, Sasank Chilamkurthy, Benoit Steiner, Lu Fang, Junjie Bai, and Soumith Chintala. Pytorch: An imperative style, high-performance deep learning library. In H. Wallach, H. Larochelle, A. Beygelzimer, F. d’Alché-Buc, E. Fox, and R. Garnett, editors, *Advances in Neural Information Processing Systems 32*. Curran Associates, Inc., 2019.
- [32] Lerrel Pinto, Marcin Andrychowicz, Peter Welinder, Wojciech Zaremba, and Pieter Abbeel. Asymmetric actor critic for image-based robot learning. *arXiv preprint arXiv:1710.06542*, 2017.
- [33] Charles R Qi, Hao Su, Kaichun Mo, and Leonidas J Guibas. Pointnet: Deep learning on point sets for 3d classification and segmentation. In *Proceedings of the IEEE conference on computer vision and pattern recognition*, pages 652–660, 2017.
- [34] Charles R Qi, Li Yi, Hao Su, and Leonidas J Guibas. Pointnet++: Deep hierarchical feature learning on point sets in a metric space. *arXiv preprint arXiv:1706.02413*, 2017.
- [35] Jiawei Ren, Xiao Ma, Chen Xu, Haiyu Zhao, and Shuai Yi. Havana: Hierarchical and variation-normalized autoencoder for person re-identification. *arXiv preprint arXiv:2101.02568*.
- [36] Mitul Saha and Pekka Isto. Manipulation planning for deformable linear objects. *IEEE Transactions on Robotics*, 23(6):1141–1150, 2007.
- [37] Jose Sanchez, Juan-Antonio Corrales, Belhassen-Chedli Bouzgarrou, and Youcef Mezouar. Robotic manipulation and sensing of deformable objects in domestic and industrial applications: a survey. *The International Journal of Robotics Research*, 37(7):688–716, 2018.
- [38] Daniel Seita, Aditya Ganapathi, Ryan Hoque, Minho Hwang, Edward Cen, Ajay Kumar Tanwani, Ashwin Balakrishna, Brijen Thananjeyan, Jeffrey Ichnowski, Nawid Jamali, et al. Deep imitation learning of sequential fabric smoothing policies. *arXiv preprint arXiv:1910.04854*, 2019.
- [39] Li Sun, Gerarado Aragon-Camarasa, Paul Cockshott, Simon Rogers, and J Paul Siebert. A heuristic-based approach for flattening wrinkled clothes. In *Conference Towards Autonomous Robotic Systems*, pages 148–160. Springer, 2013.
- [40] Eric Torgerson and Frank W Paul. Vision-guided robotic fabric manipulation for apparel manufacturing. *IEEE Control Systems Magazine*, 8(1):14–20, 1988.
- [41] Ashish Vaswani, Noam Shazeer, Niki Parmar, Jakob Uszkoreit, Llion Jones, Aidan N Gomez, Lukasz Kaiser, and Illia Polosukhin. Attention is all you need. *arXiv preprint arXiv:1706.03762*, 2017.
- [42] Petar Veličković, Guillem Cucurull, Arantxa Casanova, Adriana Romero, Pietro Lio, and Yoshua Bengio. Graph attention networks. *arXiv preprint arXiv:1710.10903*, 2017.
- [43] Nicholas Watters, Daniel Zoran, Theophane Weber, Peter Battaglia, Razvan Pascanu, and Andrea Tacchetti. Visual

interaction networks: Learning a physics simulator from video. *Advances in neural information processing systems*, 30:4539–4547, 2017.

- [44] Yilin Wu, Wilson Yan, Thanard Kurutach, Lerrel Pinto, and Pieter Abbeel. Learning to manipulate deformable objects without demonstrations. *arXiv preprint arXiv:1910.13439*, 2019.
- [45] Yuji Yamakawa, Akio Namiki, and Masatoshi Ishikawa. Motion planning for dynamic folding of a cloth with two high-speed robot hands and two high-speed sliders. In *2011 IEEE International Conference on Robotics and Automation*, pages 5486–5491. IEEE, 2011.
- [46] Wilson Yan, Ashwin Vangipuram, Pieter Abbeel, and Lerrel Pinto. Learning predictive representations for deformable objects using contrastive estimation. *arXiv preprint arXiv:2003.05436*, 2020.
- [47] Cunjun Yu, Xiao Ma, Jiawei Ren, Haiyu Zhao, and Shuai Yi. Spatio-temporal graph transformer networks for pedestrian trajectory prediction. In *European Conference on Computer Vision*, pages 507–523. Springer, 2020.
- [48] Pu Zhang, Wanli Ouyang, Pengfei Zhang, Jianru Xue, and Nanning Zheng. Sr-lstm: State refinement for lstm towards pedestrian trajectory prediction. In *Proceedings of the IEEE/CVF Conference on Computer Vision and Pattern Recognition*, pages 12085–12094, 2019.

A. Moment-Generating Function Features

For a random variable, its moment-generating function (MGF) could be used to generate its any order of moment, which fully specifies its probabilistic distribution [3]. Formally, the MGF of a random variable X with a dimension m is defined as

$$\text{MGF}_X(v) = \mathbb{E} \left[e^{v^\top X} \right] \quad (10)$$

where $v \in \mathbb{R}^m$. Eqn. 10 suggests that the MGF of a random variable X is the expectation of variable $e^{v^\top X}$.

Ma et al. [21] introduces MGF features for a set, a general-purpose learnable set feature extractor. Specifically, under the case where the distribution X is represented as an empirical distribution, i.e., $X = \{x^i\}_{i=1}^K$ where x^i is a random sample generated from $p(x)$, the MGF feature is defined as

$$\text{MGF}(\{x^i\}_{i=1}^K) = \left[\frac{1}{K} \sum_{i=1}^K x^i, \sum_{i=1}^K e^{\theta^\top x^i} \right] \quad (11)$$

where θ is a learnable weight vector. Intuitively, the MGF feature is a combination of the first order moment of the random variable X , and a set of moments specified by the parameter θ which optimized in a task-oriented manner through end-to-end training.

In G-DOOM, we consider the extracted keypoints as a sparse empirical distribution with rich features that characterizes a deformable object. Empirically, MGF features provide a better approximation to the graph and allows learning an accurate graph dynamics.

B. Graph-Based MPC

The pseudo-code of the Graph-Based MPC is given in Alg. 1. Intuitively, we initialize the search actions around each keypoints, perform K separate MPC, and output the best action with the maximum reward. For simplicity, we used the cross entropy method. A more complex solution could be considered to further improve the performance.

C. Task Details

Since the resolution of the simulation environment is different from the real-world observations, we simply use a scaling factor to make sure the depth images generated by the simulator have the same scale with real-world observations. Specifically, for an observation image with size 96×96 , the scaling factor to simulator is 70.4, which means that the corresponding covered area in the simulator is 1.36×1.36 . In NVidia-Flex, all objects are represented as a set of particles connected by springs. For all cases, we use a particle radius of 0.00625. Since the We define the reward and success condition as follows.

1) *Cloth Environments*: We randomize the initial configuration and the size of the cloth. The width and height of the cloth is sampled by $w, h \in [60, 120]$, where 60 and 120 denote the number of particles. For cloth flattening, the reward function is defined as the size of the covered area in the simulator. An episode is considered as success if $|s_t - s_{\max}| < 0.08$, where s_t is the current size and s_{\max} is the maximum covered size of the object. For cloth folding, the reward is defined as the average distance between the two halves of the particles. If the distance is smaller than 0.05, then the episode is considered as a success.

2) *Rope Environment*: We randomize the rope length by $l \in [40, 50]$, where 40 and 50 denote the number of particles. For each task, we define the goal position of the two ends (e_g^1, e_g^2) of the rope to specify the destination configurations. Given the current position of two ends (e^1, e^2) , if $\|e^1 - e_g^1\|_2 + \|e^2 - e_g^2\|_2 < 0.05$, we consider the task to be a success.

3) *Real Robot Metrics*: In our real robot experiments, since it is difficult to measure the success rate, we compute reward, which is defined over the pixel space. Specifically, we define the reward for cloth flattening task as $r = |S_{\text{cloth}}|$ where S_{cloth} denotes the set of pixels covered by cloth, and define the reward for cloth folding task as the $r = -\left| |S_{\text{cloth}}| - \frac{|S_{\text{flatten}}|}{2} \right|$, where S_{flatten} denotes the flattened area. For rope flatten environments, we define the reward as $r = |S_{\text{rope}} \cap S_{\text{goal}}|$, where S_{goal} is the goal region defined for each task. For each task where the observation has a width 400, the goal region has a width of 30 pixels. Visualizations of the goal regions of rope straightening tasks are provided in Fig. 8

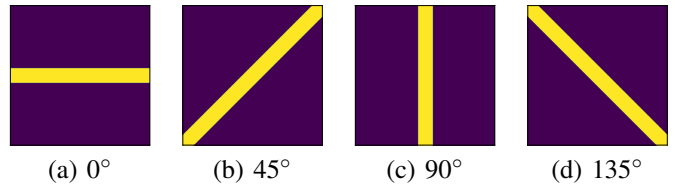


Fig. 8. The goal region of rope straightening tasks in the real robot setup.

D. Implementation Details

We implement G-DOOM with PyTorch [31] and train all models on NVidia RTX 2080Ti GPUs.

1) *Transporter Networks*: A Transporter network consists of two main components: feature extractor f_{enc} , keypoint detector f_{kp} , and a decoder f_{dec} . For a clean notation, we first define a convolutional layer as $\text{Conv}(C, J, S, P)$, where C is the channel number, J is the kernel size, S is the stride, and P is the padding size. We use a feature extractor with shape: $[\text{Conv}(32, 7, 1, 3), \text{Conv}(32, 3, 1, 1), \text{Conv}(64, 3, 1, 1), \text{Conv}(64, 3, 1, 1), \text{Conv}(128, 3, 2, 1)]$. f_{kp} shares the same structure with f_{enc} , followed by an additional layer $\text{Conv}(K, 1, 1, 0)$, which regresses for K keypoints. The decoder f_{dec} is the reverse of the encoder, with two additional bilinear upsampling layer with a factor of 2 to scale up the feature map size. After all layers, ReLU activation is used.

Algorithm 1: Graph-Based MPC

Input: current observation I_t , previous belief h_{t-1} , planning horizon H , optimization iterations I , candidates per iteration J , number of top candidates C , transition model ($\{v_t^i\}_{i=1}^K, h_t) = f_d(\{v_{t-1}^i\}_{i=1}^K, h_{t-1}, a_{t-1})$, reward model $\tilde{r} = f_r(\{v_t^i\}_{i=1}^K)$
 $\{v_t^i\}_{i=1}^K, \{p_t^i = (x_t, y_t)\}_{i=1}^K \leftarrow \text{Transporter}(I_t)$
Initialize action sequence distributions around keypoint k as $p^k(a_{t:t+H}(k)) \leftarrow \mathcal{N}(\mu(k) = [x_t^k, y_t^k, x_t^k, y_t^k], \mathbb{I})$
// The following process could be paralleled using GPU which gives no overhead to the algorithm
for optimization iteration $n = 1 \dots I$ **do**
 for keypoint $k = 1 \dots K$ **do**
 for candidate action sequence $j = 1 \dots J$ **do**
 $a_{t:t+H}^j(k) \sim q^k(a_{t:t+H}(k))$
 $(\{v_{t+1:t+H+1}^i(k)\}_{i=1}^K, h_{t+1:t+H+1}(k)) = f_d(\{v_t^i\}_{i=1}^K, h_t, a_{t:t+H}(k))$
 $R^j(k) = \sum_{\tau=t+1}^{t+H+1} f_r(\{v_{\tau:t+H+1}^i(k)\}_{i=1}^K)$
 end
 // re-fit the action distribution to the C best action sequences.
 $\mathcal{C}(k) \leftarrow \text{argsort}(\{R^j(k)\}_{j=1}^J)_{1:C}$
 $\mu_{t:t+H}(k) = \frac{1}{C} \sum_{c \in \mathcal{C}(k)} a_{t:t+H}^c$
 $\sigma_{t:t+H}(k) = \frac{1}{C-1} \sum_{c \in \mathcal{C}(k)} |a_{t:t+H}^c - \mu_{t:t+H}(k)|$
 $q(a_{t:t+H}(k)) = \mathcal{N}(\mu_{t:t+H}(k), \sigma_{t:t+H}(k)^2 \mathbb{I})$
 end
end
 $\mu_{\max} = \text{argmax}_{\mu_{t:t+H}(k)} R^J(k)$
Output: the first action mean μ_t of μ_{\max}

2) *Recurrent Graph Dynamics:* The recurrent dynamics consists of three components: the TGConv for graph interaction modeling, MGF for set feature extraction, and a RNN for belief update. The TGConv takes in the concatenation of previous belief h_{t-1} , current graph features $\{v_t^i\}_{i=1}^K$, current action a_t as input. Here, v_t^i and h_t are vectors of length 200, and a_t is embedded into a vector of length 32 by a fully connected layer. After concatenation, they are further embedded by a fully connected layer into a vector of size 200, then passed through a standard TGConv of 2 layers. In the MGF feature extractor, we use a matrix with size $[200, 200]$, i.e., we extract 200 moments as additional information. For RNN, we use a standard GRU with a hidden state size of 200. After all layers, ReLU activation is used.

3) *Contrastive Learning Setups:* For each positive sample (\tilde{v}_t, v_t) , we randomly sample 50 irrelevant encoded states v_n as the negative samples.

4) *Model Learning:* For all models, we use Adam optimizer with a learning rate of 0.0003. We first train the Transporter network, freeze the weights, and train the contrastive dynamics.

5) *Real Robot Setups:* For our robot experiments, we use a Kinova Gen3 robot with Robotiq gripper. A top-down Kinect 2 camera is used to capture the depth images. To improve the quality of depth images and minimize the sim-to-real gap, we normalize the depth values to match with the simulation environment, and perform image denoising with a simple convolutional kernel. For simplicity, we compute the segmentation mask of the object by converting the RGB image observation to HSV color space, and apply a high pass filter over the color values, which selects the green pixels. We

find this simple trick works well in practice. To generalize better to different scenarios, a neural network based foreground segmentor can be considered. We leave it for future study. The height of grasping is determined by estimating the height of objects with the detected point cloud from Kinect. Specifically, we estimate 5 times and take the average as the final output, which we observe to improve the success rate.

E. Additional Results

1) *Detail Rewards:* We report the detailed reward achieved in each task. Specifically, we also compare with one of the SOTA off-policy model-free reinforcement learning method, Soft Actor-Critic (SAC), as a reference. Note that the SAC is trained for the same number of steps as the model-based methods. The difference is that for model-based methods in the main text, we use a random policy to initialize the dataset, and directly fit the model using the randomly generated data. For SAC, we interact with the environment and collect data using the learned actor. The detailed results are given in Tab. V.

TABLE V
SIMULATION EXPERIMENT: REWARD

	Rope				Cloth	
	0°	45°	90°	135°	Flatten	Fold
SAC	-0.415	-0.462	-0.339	-0.292	0.142	-0.161
CFM	-0.193	-0.239	-0.275	-0.266	0.162	-0.198
PlaNet	-0.158	-0.129	-0.135	-0.107	0.197	-0.181
G-DOOM	-0.138	-0.114	-0.124	-0.092	0.252	-0.139

We observe that G-DOOM achieves the highest reward in all task. In particular, SAC works worse than the model-based

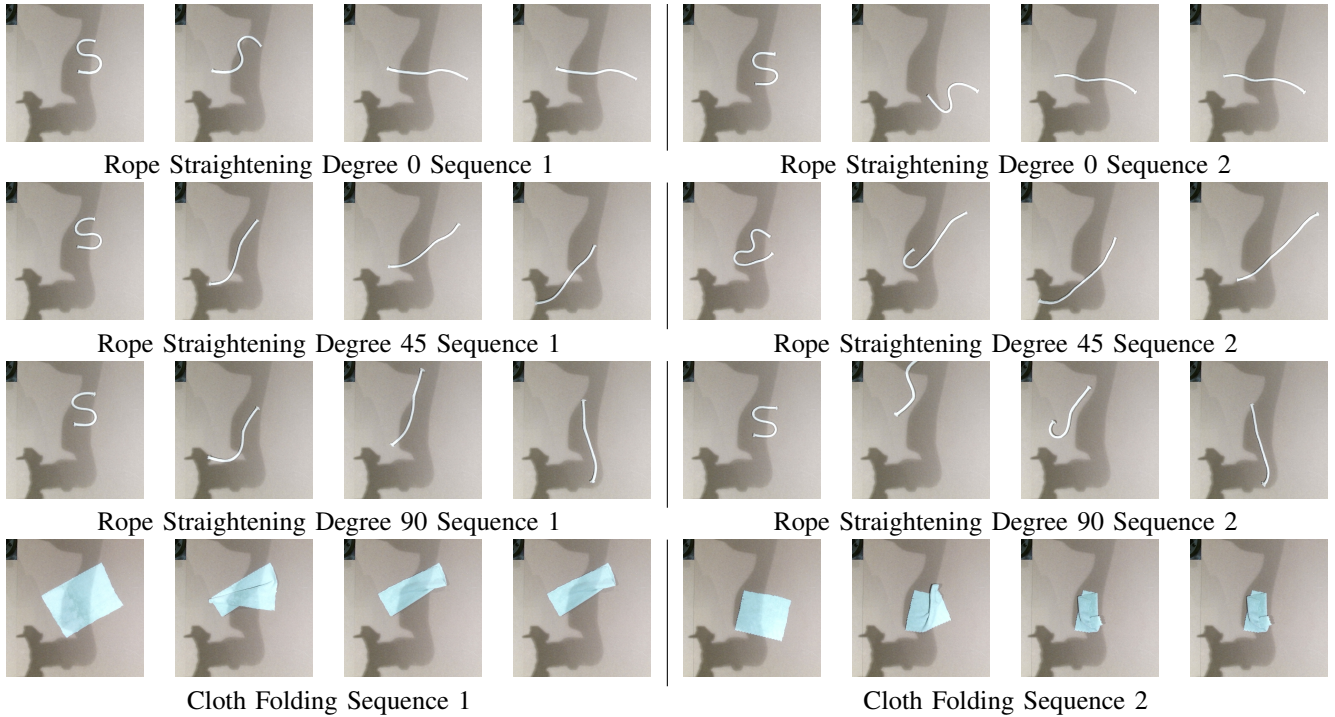


Fig. 9. Additional visualizations of the real robot G-DOOM experiments.

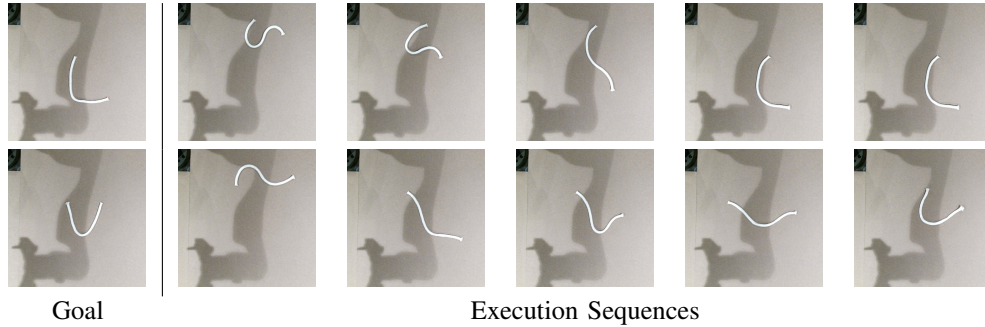


Fig. 10. Goal-oriented rope manipulation experiments.

methods in most cases. This is expected since for a model-free method, 5000 episodes is insufficient for learning a good policy. The performance of SAC is possible to improve given longer training time. However, since the NVidia-Flex simulator is slow to run, training for longer steps is difficult. In addition, it is hard for SAC to achieve goal-specific planning, which is common for the model-based methods. Thus, we only use SAC as a reference. In addition, we also provide the detailed rewards of the ablations in Tab. VI. G-DOOM achieves the highest reward among all variants.

F. Additional Visualizations

In the main text, we only provide visualizations of cloth flattening and rope straightening degree 135° due to space limit. We present additional visualizations of the real robot experiments of G-DOOM in Fig. 9. Note that for cloth flattening and rope straightening degree 0, since the task finishes within 3 steps, we repeat the last two frames for alignment consideration.

TABLE VI
ABLATION STUDY: REWARD

	Rope				Cloth	
	0°	45°	90°	135°	Flatten	Fold
NoGraph	-0.262	-0.286	-0.312	-0.162	0.233	-0.186
NoRNN	-0.176	-0.150	-0.136	-0.111	0.232	-0.306
NoContrastive	-0.441	-0.406	-0.394	-0.350	0.178	-0.296
InfoNCE	-0.313	-0.124	-0.213	-0.252	0.165	-0.207
CEM	-0.216	-0.129	-0.159	-0.161	0.245	-0.211
GAT	-0.238	-0.285	-0.198	-0.185	0.187	-0.277
MaxPool	-0.191	-0.172	-0.174	-0.123	0.252	-0.190
G-DOOM	-0.138	-0.114	-0.124	-0.092	0.252	-0.139

In addition, the results for goal-oriented rope manipulation is provided in Fig. 10. With the contrastively trained dynamic model, G-DOOM can be easily applied for goal-oriented rope manipulation. However, it remains difficult for cloth manipulation that requires careful 3D understanding. We leave it for future study.